

Sunlight Powered Multi-Energy Complementary Utilization System for CO₂ Recycling Based on Concentrating Spectral Splitting Strategy

Junyan He¹, Kai Zhang¹, Yimin Xuan^{1*}

¹ School of Energy and Power Engineering, Nanjing University of Aeronautics and Astronautics, Nanjing 210016, China (* Corresponding Author)

ABSTRACT

A sunlight driven multi-energy complementary utilization system based on concentrating spectral beam splitting strategy is proposed for CO₂ recycling. The high-energy shortwave part of solar spectrum is converted into electricity by photovoltaic cells to activate water electrolysis reaction for H₂ production, while the residual energy is transformed into heat by an evacuated heat-collecting tube to trigger the decomposition of saturated CO₂ adsorbents. Subsequently, the released CO₂ reacts with the previously generated H₂ to form fuel, realizing autothermic CO₂ conversion. Thermodynamic analysis of this model system reveals that the optimized solar-to-methane efficiency and heat-collecting efficiency could reach up to 8.08% and 68.79% respectively, when the splitting waveband for photovoltaics-water electrolysis is 600-900 nm. The current work provides a viable solution for the short-term implementation of solar-driven CO₂ conversion technology into large-scale energy markets.

Keywords: full spectrum utilization, carbon dioxide conversion, splitting waveband, solar-to-fuel efficiency

1. INTRODUCTION

Fossil fuels burning has led to severe energy shortage and notorious climate issues. Improving the utilization of renewable energy while also reducing carbon dioxide emissions becomes the only way to achieve a sustainable development of human society.

Among various kinds of renewable energy, widely-distributed solar energy [1] has an absolute advantage, with an increasing on photovoltaics [2] and photo-thermal [3] applications more than ever. However, both the above energy utilization strategies have their own shortcomings, resulting in the insufficient utilization of

solar energy. For instance, solar cells can only adsorb the photons with energy larger than their inherent bandgaps, resulting in the waste of energy from long wavelength photons into heat, which will be detrimental to their performance stabilities [4]. While for the photo-thermal devices, solar energy is completely converted into heat, regardless of the difference in energy quality carried by photons. Accordingly, cascading utilization of the full-spectrum solar energy by means of concentrating spectral-splitting technology has attracted tremendous attention in recent years. Coventry [5], as a case in point, early proposes a medium-concentration parabolic trough photovoltaics/thermal collector, which reuses the flux of waste heat on the cells and improves electrical efficiency to 11% with 58% thermal efficiency measured under typical operating conditions. Furthermore, Gur et al. [6] point out the superior performance of a concentrating photovoltaics/thermal system which can produce electricity and thermal energy simultaneously at high temperature under various economic conditions. More recently, Qu et al. [7] design a spectral splitting concentrator with a two-layer mirror and realize a 19% total conversion efficiency by integrating photovoltaics and solar thermochemical processes under a low concentrating condition, guaranteeing the operational stability of solar cells as wells as generating hydrogen energy.

CO₂ capture, utilization and storage, refers to the set of technologies for trapping the carbon emissions, storing them underground or using them for a range of industrial applications. Among the currently reported technologies, sunlight driven CO₂ recycling is considered as the most promising solution to mitigate global emissions. Hence, there has been an explosive growth in researches focused on the direct CO₂ conversion driven by solar energy recently, typically like photocatalytic [8],

Selection and peer-review under responsibility of the scientific committee of the 13th Int. Conf. on Applied Energy (ICAE2021).

Copyright © 2021 ICAE

photo-thermal [9], and photoelectrochemical [10] CO₂ reduction. Nonetheless, their current efficiencies are still too low for practical applications.

Here in this work, we propose a solar energy cascade utilization system for CO₂ recycling, via the integration of several commercialized technologies. By means of concentrating spectral splitting technology, the high energy part of solar spectrum is applied for photovoltaics to drive water splitting while the residue part is converted into heat to trigger the decomposition of saturated CO₂ adsorbents. Afterwards, the H₂ produced from water electrolysis reacts with the released CO₂, ultimately leading to the formation of hydrocarbon fuels and achieving autothermic conversion of CO₂ as well. We also perform a systemic thermodynamic analysis on this model system, further verifying the feasibility of this technology in large-scale energy markets.

2. SYSTEM MODEL

2.1 Operating principle

The schematic diagram of the sunlight powered multi-energy complementary utilization system is shown in Figure 1. The solar energy conversion unit is composed of a spectral splitting parabolic trough collector, photovoltaics cells with heat sinks bellow, and a heat-collecting reaction tube above, prefilled with saturated CO₂ adsorbents in the front section and activated catalysts in an adiabatic section behind (Figure 2).

At night or on a cloudy day, adsorbents are exposed to flue gas to capture and purify CO₂. Relatively, when sun shines on the concentrator, a part of high-energy shortwaves is split up via the splitter and reflected on photovoltaic cells to output electricity. Later, output power directly drives water electrolyzer to generate H₂. The remaining parts of sunlight are transmitted to the front section of the tube above, in which saturated CO₂ adsorbents absorb heat from solar beams to desorb CO₂. Subsequently, a mixture of the released gaseous CO₂ and the previously generated H₂ carrying sensible heat, flows through the porous fixed catalytic bed behind, and finally converts into fuel.

Further, several heat sinks and exchangers are set in the system to promote heat-collecting efficiency. Underneath photovoltaic cells, the heat sinks utilize water to recover the low-temperature waste heat emitted by cells, and keep cells operating well. Next, the heat collected via water is transferred into a heat exchanger to preheat H₂. Besides, in the outlet of the reaction tube, the other heat exchanger uses outlet gas temperature to preheat H₂ again. In this way, inlet

temperature of the tube is promoted greatly before solar heat comes into use, which leads to reductions in reaction temperature difference, as well as unnecessary energy consumption.

2.2 Theoretical calculation

To illustrate the process of energy transmission and transformation, five submodules, as well as the solar-to-fuel efficiency calculation equation are expanded as follows.

2.2.1 Incident energy module

Total energy picked up by the photovoltaic cells as well as reaction tube is described as [11]

$$E_{in,PV} = C_{geo,PV} \cdot \eta_{opt,PV} \cdot \left(\int_{\lambda_1}^{\lambda_2} E(\lambda) d\lambda \cdot A_{d,PV} + \int_{280}^{4000} E(\lambda) d\lambda \cdot A_{c,PV} \right) \quad (1)$$

$$E_{in,TH} = C_{geo,TH} \cdot \eta_{opt,TH} \cdot \left(\int_{280}^{\lambda_1} E(\lambda) d\lambda + \int_{\lambda_2}^{4000} E(\lambda) d\lambda \right) \cdot A_{d,g} \quad (2)$$

where $C_{geo,PV} = 10$, $C_{geo,TH} = 20$ are geometric concentration ratio of photovoltaics and tube; $\eta_{opt,PV} = 0.75$, $\eta_{opt,TH} = 0.70$ are the optical efficiency of photovoltaics and tube; $E(\lambda)$ is the solar spectral irradiance from AM 1.5D, W/(m²·nm); $A_{c,PV}$, $A_{d,PV} = 0.2448$ m² are the areas of cells in two sections; $A_{d,g} = 0.07\pi$ m² is the surface area of CO₂ desorption section of the tube.

2.2.2 Photovoltaics-water electrolysis energy module

On the surface of photovoltaic cells, a part of Joule heat derived from received energy is lost via heat radiation and natural convection, expressed as [11]

$$Q_{loss,PV} = \varepsilon_{PV} \sigma (T_{PV}^4 - 290^4) \cdot A_{PV} + h_{PV} (T_{PV} - 298) \cdot A_{PV} \quad (3)$$

where $\varepsilon_{PV} = 0.85$ is the surface emissivity; $\sigma = 5.67 \times 10^{-8}$ W/(m²·K⁴) is Stefan-Boltzmann constant; $T_{PV} = 303$ K is the average temperature of cells; $h_{PV} = 4.8$ W/(m²·K) is heat transfer coefficient.

Since the conversion efficiency of solar cells is affected by incident intensity, it needs to be recalculated, and corresponding output power is expressed as [12]

$$P_{PV} = \eta_{d,PV} \cdot \int_{\lambda_1}^{\lambda_2} E(\lambda) d\lambda \cdot A_{d,PV} \cdot N_{d,PV} \cdot C_{geo,PV} \cdot \eta_{opt,PV} \cdot \eta_{mode} + \eta_{c,PV} \cdot \int_{280}^{4000} E(\lambda) d\lambda \cdot A_{c,PV} \cdot N_{c,PV} \cdot C_{geo,PV} \cdot \eta_{opt,PV} \cdot \eta_{mode} \quad (4)$$

where $\eta_{c,PV} = 0.22$, $\eta_{d,PV} = 0.31$ are the efficiency of one concentrated m-Si cell [11]; $N_{c,PV}$, $N_{d,PV} = 16$ are cell numbers; $\eta_{mode} = 0.9$ is the component loss of photovoltaic module.

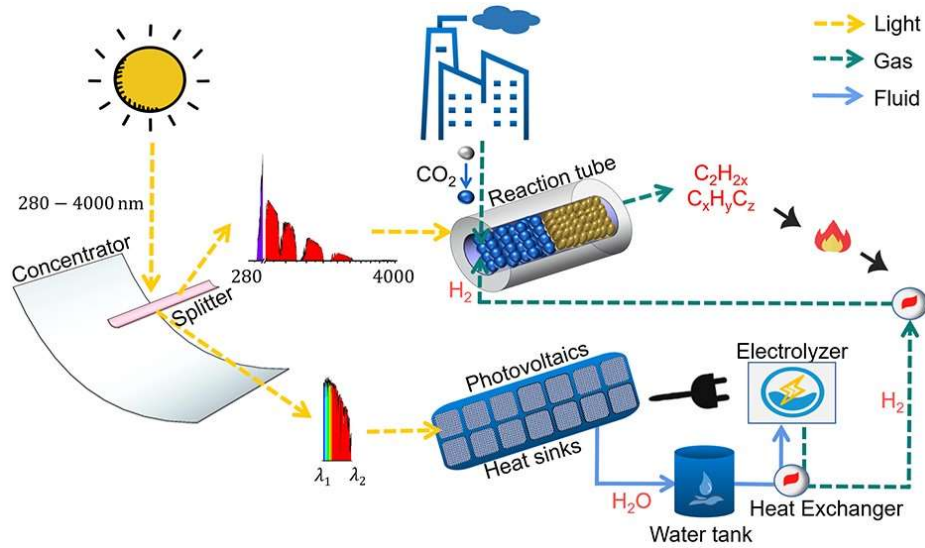


Fig. 1. The schematic diagram of sunlight powered multi-energy complementary utilization system

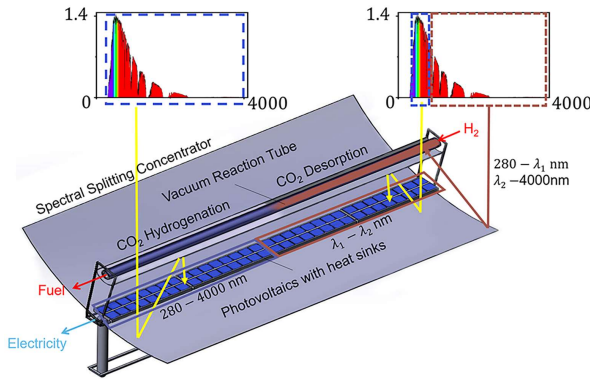


Fig. 2. Diagram of the solar energy conversion unit

Joule heat can also be carried out by water to exchange heat. Hence, the heat for low-temperature heat exchange is expressed as

$$Q_{cool,PV} = h_{d,H_2O} \cdot \Delta T_{d,cool} \cdot A_{d,PV} + h_{c,H_2O} \cdot \Delta T_{c,cool} \cdot A_{c,PV} \quad (5)$$

where $h_{c,H_2O} = 300 \text{ W}/(\text{m}^2 \cdot \text{K})$, $h_{d,H_2O} = 500 \text{ W}/(\text{m}^2 \cdot \text{K})$ are the heat transfer coefficient; $\Delta T_{c,cool}$, $\Delta T_{d,cool}$ are the water temperature difference, can be calculated combining with the effective area of heat exchanger based on Fourier Law and energy balance equation.

Balance of total, available and unavailable energy on photovoltaic cells can be expressed as

$$E_{in,PV} = P_{PV} + Q_{loss,PV} + Q_{cool,PV} \quad (6)$$

2.2.3 Water-electrolysis module

A commercial electrolyzer which can highest achieve 600 ml H_2 per minute at 30 A current, is used in the model analysis. According to standard requirements on commercial electrolyzer, the molar flow of H_2 is

determined by effective input power, and related equation is written as [13]

$$n_{H_2} = V_{H_2}^0 \cdot \frac{P_{PV}}{V_{cha}} \cdot \eta_{ELE} \quad (7)$$

where $V_{H_2}^0 = 0.000418 \text{ m}^3/(\text{A} \cdot \text{h})$ is the volume of H_2 produced by one quantity of electric charge per channel; $V_{cha} = 2.2 \text{ V}$ is the decomposition voltage per channel; $\eta_{ELE} = 1$ is Faraday efficiency of water electrolysis.

2.2.4 CO_2 capture energy module

Heat loss occurs in CO_2 desorption section, including heat conduction between tube walls, natural convection between walls and fluid or air, and radiation between tube and sky, expressed as [11]

$$Q_{loss,TH} = Q_{cond,TH} + Q_{conv,TH} + Q_{rad,TH} \quad (8)$$

$$Q_{cond,TH} = \frac{k_g \cdot \Delta T_g}{r_g \cdot \ln\left(\frac{r_g + \delta_g}{r_g}\right)} \cdot A_{d,g} + \frac{k_s \cdot \Delta T_s}{r_s \cdot \ln\left(\frac{r_s + \delta_s}{r_s}\right)} \cdot A_{d,s} \quad (9)$$

$$Q_{conv,TH} = h_{air} (T_{des} - 290) \cdot A_{d,g} + h_{H_2} (T_{des} - T_{H_2}) \cdot A_{d,s} \quad (10)$$

$$Q_{rad,TH} = \varepsilon_d \cdot \sigma (T_{des}^4 - 290^4) \cdot A_{d,g} \quad (11)$$

where $k_g, k_s = 5 \text{ W}/(\text{m} \cdot \text{K})$ are thermal conductivity; $\Delta T_g = 2 \text{ K}$, $\Delta T_s = 5 \text{ K}$ are temperature difference between inner and outer walls of glass and stainless tubes; r_g, r_s are the radius of glass and stainless tubes, m; δ_g, δ_s are the thickness of tube walls, m; $h_{air} = 12 \text{ W}/(\text{m}^2 \cdot \text{K})$ is natural convection transfer coefficient; $h_{H_2} = 10 \text{ W}/(\text{m}^2 \cdot \text{K})$ is convection coefficient in the tube; T_{des} is desorption temperature, K; T_{H_2} is hydrogen inlet temperature evaluated by shortcut

method, K ; $A_{d,g} = 0.07\pi \text{ m}^2$, $A_{d,s} = 0.0384\pi \text{ m}^2$ are the surface areas of glass and stainless tubes in CO_2 desorption section; $\varepsilon_d = 0.08$ is surface emissivity.

Balance of total, available and wasted energy in photochemical stage is written as

$$E_{in,TH} = E_{in,TH,C} + Q_{loss,TH} \quad (12)$$

Viewing CO_2 desorption section as a steady equilibrium state, the energy balance inside is described as [14]-[15]

$$E_{in,TH,C} = c_{m,H_2} \cdot n_{H_2} \cdot (T_{des} - T_{H_2}) + n_{CO_2} \cdot \Delta H_{des} \quad (13)$$

$$c_{m,H_2} = 28.80247 + 0.00307T_{H_2} - 4.37556 \times 10^{-6} T_{H_2}^2 \quad (14)$$

$$n_{CO_2} = (1 - \varepsilon_{d,bed}) \cdot \rho_d \cdot 2475 e^{\frac{11237}{T_{des}}} \cdot V_{d,s} \quad (15)$$

where c_{m,H_2} is molar heat capacity of H_2 , $\text{J}/(\text{mol}\cdot\text{K})$; n_{CO_2} is molar flow rate of CO_2 , mol/s ; ΔH_{des} is the enthalpy change of desorption, J/mol ; $\varepsilon_{bed,d} = 0.7$ is the porosity of desorption bed; $\rho_d = 2840 \text{ kg}/\text{m}^3$ is the density of K-promoted hydrotalcites sorbents; $V_{d,s} = 0.0192^2\pi \text{ m}^2$ is the volume of tube in CO_2 desorption section.

2.2.5 CO_2 conversion reaction module

Since CO_2 hydrogenation part is adiabatic, heat loss is ignored, and the energy balance inside catalysis section can be described as [15]

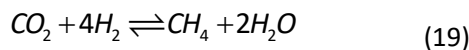
$$Q_{sen} + Q_{cat} = 0 \quad (16)$$

$$Q_{sen} = c_{m,mix} \cdot (n_{H_2} + n_{CO_2}) \cdot (T_{cat} - T_{des}) \quad (17)$$

$$Q_{cat} = R_{fuel} \cdot V_{c,s} \cdot \Delta H_{cat} \quad (18)$$

where $c_{m,mix} = 30.50673 + 0.01476T_{des} - 1.83887 \times 10^{-5} T_{des}^2$ is taken from the material library in COMSOL Multiphysics® 5.6, $\text{J}/(\text{mol}\cdot\text{K})$; T_{cat} is catalysis temperature, K ; R_{fuel} is fuel production rate, $\text{mol}/\text{m}^3/\text{s}$; $V_{c,s} = 0.0192^2\pi \text{ m}^2$ is the volume of tube in catalysis section; ΔH_{cat} is the enthalpy change of catalysis, J/mol .

Under atmosphere pressure, it is much easier to convert CO_2 into methane when operating the system. The chemical equation and enthalpy change is written as [16]



$$\Delta H_{CH_4} = -\frac{4.18}{1000} \left(16.4T_{cat} - 0.00557T_{cat}^2 + \frac{112000}{T_{cat}} + 34633 \right) \quad (20)$$

In the system, the yield of fuel is modeled by reaction kinetics. Refer to the experiment data from Miguel et al

[17], reaction kinetic equation of CO_2 methanation over Ni-based catalysts at 473-673 K, is written as

$$R_{CH_4} = (1 - \varepsilon_{c,bed}) \cdot \rho_c \cdot \left[\frac{k p_{CO_2}^{0.5} p_{H_2}^{0.5}}{(1 + K_{OH} \frac{p_{H_2O}}{p_{H_2}^{0.5}})^2} \cdot \left(1 - \frac{p_{fuel} p_{H_2O}^2}{p_{CO_2} p_{H_2}^4 K_{eq}} \right) \right] \quad (21)$$

$$k = 0.008936 e^{\left[-14275 \left(\frac{1}{T_{cat}} - \frac{1}{300} \right) \right]} \quad (22)$$

$$K_{OH} = 0.4326 e^{\left[-7414 \left(\frac{1}{T_{cat}} - \frac{1}{300} \right) \right]} \quad (23)$$

$$K_{eq} = e^{\left[\frac{1.0}{1.987} \left(\frac{56000}{T_{cat}} + \frac{34633}{T_{cat}} - 16.4 \ln(T_{cat}) + 0.00557 T_{cat} \right) + 33.165 \right]} \quad (24)$$

where $\varepsilon_{bed,c} = 0.52$ is the porosity of catalysis bed; $\rho_c = 1875 \text{ kg}/\text{m}^3$ is the density of catalysts; k is reaction rate constant, $\text{mol}/(\text{g}\cdot\text{s}\cdot\text{Pa}^{0.5})$; K_{OH} is adsorption equilibrium constant, $\text{Pa}^{-0.5}$; K_{eq} is reaction equilibrium constant, Pa^{-2} ; p_{gas} is partial pressure based on Dalton's Law, Pa .

A parameter U related to gas concentration C is adopted to verify the reaction is under thermodynamic limit.

$$U = \frac{(C_{CH_4})(C_{H_2O})^2}{(C_{CO_2})(C_{H_2})^4} < K_{eq} \quad (25)$$

2.2.6 Solar-to-fuel efficiency

Solar-to-fuel efficiency is taken as an evaluation index for this solar-driven CO_2 recycling system model, which is expressed as

$$\eta_{solar-to-fuel} = \frac{n_{fuel} \cdot LHV_{fuel}}{\int_{280}^{4000} E(\lambda) d\lambda \cdot A_{con}} \quad (26)$$

where LHV_{fuel} is low heat value of fuel, J/mol ; $A_{con} = 5 \text{ m}^2$ is the effective area of the concentrator.

3. RESULTS AND DISCUSSION

3.1 Influence of splitting waveband on solar-to-fuel efficiency

Figure 3(a) shows the distribution of desorption temperature, seen as the initial condition of catalysis process. Then, catalysis process maintains in an appropriate reaction state thanks to its exothermic characteristic, of which the temperature is equal to or even higher than the desorption temperature ahead, as shown in Figure 3(b). Varying with splitting wavebands, the temperature is fluctuating, up to 650 K.

Figure 3(c) shows how solar-to-fuel efficiency changes with splitting wavebands, in which the scope of λ_1 belongs to 400-600 nm, and λ_2 is 600-900 nm. Figure 3(d) shows the data verification, in which only four data points are above the thermodynamic limit and thus are deleted, to guarantee the model accuracy.

In a relatively wide splitting waveband, while solar energy put into saturated CO_2 adsorbents desorption process is too little to produce CO_2 , the residual energy reflected to cells is too much to completely convert H_2 , so solar-to-fuel efficiency is surely lower. Instead, a narrower waveband may comparatively show a better result but still depends on the balance of energy partition in photovoltaics-water electrolysis H_2 production and CO_2 desorption and methanation. Through data analysis, 8.08% solar-to-fuel efficiency, also the highest, appears in 600-900 nm splitting waveband. Additionally, under this condition, both desorption and catalysis temperature are 520-537 K.

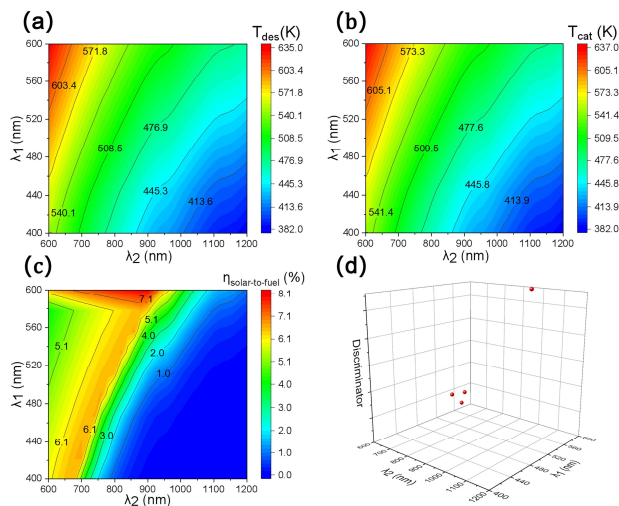


Fig. 3. Simulated values of: (a) catalysis temperature, (b) desorption temperature, (c) conversion efficiency, (d) data verification

3.2 Distribution characteristics of energy loss

On the condition of 600-900 nm splitting waveband for photovoltaics, Figure 4 depicts the energy transfer process of the typical model. Irreversible heat loss is about 35.21%, and total heat-collecting efficiency reaches to 64.79%. As a result, solar-to-methane efficiency can get to 8.08%. As designed, the low-temperature and middle-temperature waste heat can be reused to preheat reactants. Undoubtedly, the more waste heat is reused, the higher solar-to-fuel efficiency is. In contrast to other splitting system under the same concentration ratio [7], energy loss reduces by 27.69%.

4. CONCLUSIONS

In this paper, a multi-energy complementary utilization system for CO_2 recycling with net-zero carbon emission based on concentrating spectral splitting strategy is proposed. Solar energy is appropriately allocated to photovoltaics-water electrolysis for H_2 production and photo-thermal CO_2 desorption from adsorbents. Further, the released CO_2 reacts with the generated H_2 to form hydrocarbon fuels by self-heating. In a typical model to prepare CH_4 , solar-to-fuel efficiency and total heat recovery reach up to 8.08% and 64.79% respectively when 600-900 nm waveband is for photovoltaics-water electrolysis. The system is promising in realizing clean, low-consumption and efficient CO_2 recycling driven by full-spectrum solar energy.

ACKNOWLEDGEMENT

The authors gratefully acknowledge financial support from the Basic Science Center Program for Ordered Energy Conversion of the National Natural Science Foundation of China (No. 51888103).

REFERENCE

- [1] Ju X, Xu C, Liao ZR, et al. A review of concentrated photovoltaic-thermal (CPVT) hybrid solar systems with waste heat recovery (WHR). *Science Bulletin* 2017;62(20):1388-1426.
- [2] Lee YS, Park CL, Balaji N, et al. High-efficiency Silicon Solar Cells: A Review. *Israel Journal of Chemistry* 2015;55(10):1050-1063.
- [3] Shi L, Wang XZ, Hu YW, et al. Solar-thermal conversion and steam generation: a review. *Applied Thermal Engineering* 2020;179:1-14.
- [4] Shockley W, Queisser HJ. Detailed Balance Limit of Efficiency of PN Junction Solar Cells. *Journal of Applied Physics* 1961;32:510-519.
- [5] Coventry JS, Performance of a Concentrating Photovoltaic/Thermal Solar Collector, *Sol. Energy* 2005;78(2):211-222.
- [6] Gur M, Abraham K, Abraham D. Solar cooling with concentrating photovoltaic/thermal (CPVT) systems. *Energy Conversion and Management* 2007;48(9):2481-2490.
- [7] Qu WJ, Hong H, Jin HG. A spectral splitting solar concentrator for cascading solar energy utilization by integrating photovoltaics and solar thermal fuel. *Applied Energy* 2019;248:162-173.
- [8] Francis A, S. SP, S HK, et al. A review on recent developments in solar photoreactors for carbon dioxide conversion to fuels. *Journal of CO2 Utilization* 2021;47:1-19.

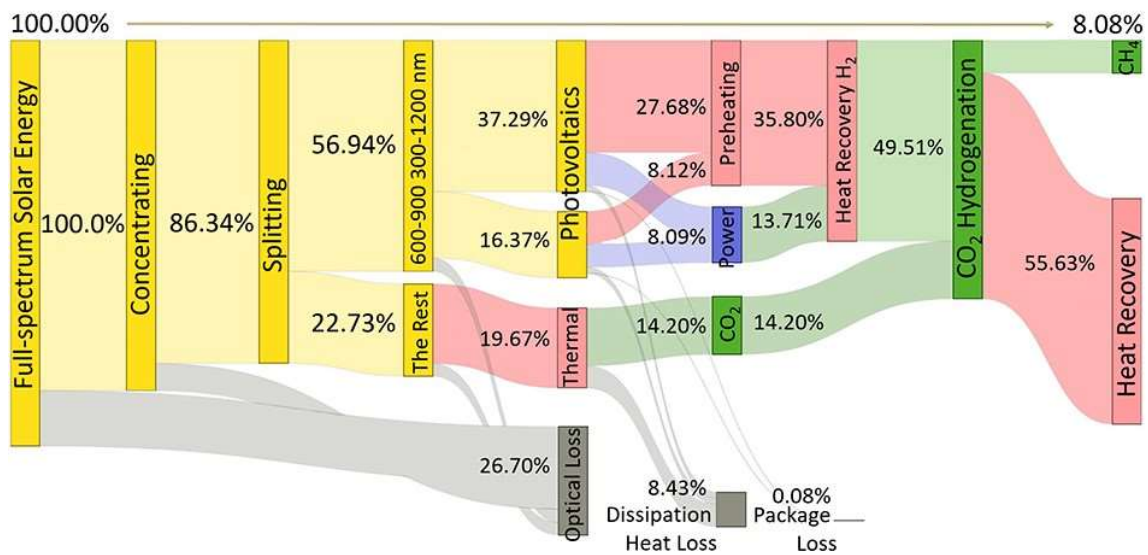


Fig. 4. Sankey diagram of the typical model

[9] Liu JX, Li YJ, Liu HM, et al. Photo-thermal Synergistically Catalytic Conversion of Glycerol and Carbon Dioxide to Glycerol Carbonate over Au/ZnWO₄-ZnO Catalysts. *Applied Catalysis B: Environmental* 2018;244:836-843.

[10] Chen XP, Zhang ZX, Chi L, et al. Recent Advances in Visible-Light-Driven Photoelectrochemical Water Splitting: Catalyst Nanostructures and Reaction Systems. *Nano-Micro Letters* 2016;8(01):1-12.

[11] Wang YJ, Li Q, Li DH, et al. Thermodynamic Analysis for a Concentrating Photovoltaic-thermochemical Hybrid System. *Journal of Engineering Thermophysics* 2018;39(05):1021-1026.

[12] Ju X, Wang Z F, Flamant G, et al. Numerical analysis and optimization of a spectrum splitting concentration photovoltaic-thermoelectric hybrid system. *Solar Energy* 2012;86(6):1941-1954.

[13] ISO 22734: Hydrogen generators using water electrolysis process - Part 1: Industrial and commercial applications; 2019.

[14] Zhu YS, Cai N. High-pressure carbon dioxide adsorption kinetics of potassium-modified hydrotalcite at elevated temperature, *Fuel* 2017;207:579-590.

[15] Du WP, Lee MT, Wang YF, et al. Design of a solar-driven methanol steam reforming receiver/reactor with a thermal storage medium and its performance analysis. *International Journal of Hydrogen Energy* 2020;45(58):33076-33087.

[16] Forsythe RK, Verostko CE, Cusick RJ, et al. A Study of Sabatier Reactor Operation in Zero "G". *SAE Technical Paper 840936* 1984;1:1-8.

[17] Miguel CV, Mendes A, Madeira LM. Intrinsic kinetics of CO₂ methanation over an industrial nickel-based catalyst. *Journal of CO₂ Utilization* 2018;25:128-136.